

1 **Estimating the impact of a major hurricane on**
2 **transport processes**

3 Thomas Dobbelaere, Emmanuel Hanert

4 February 22, 2021

5 **Abstract**

6 In most hydrodynamic model studies, currents and waves are simu-
7 lated separately. This is especially true for the simulation of passive
8 drifters, whose trajectories are often computed based solely on cur-
9 rents. Although this simplification holds for most situations, as the force
10 exerted by waves on currents can be neglected in fair weather condi-
11 tions, it may lead to significant errors during storm conditions, when
12 currents are strongly influenced by wind-generated waves. In this study,
13 we investigate current-wave interactions in heavy-wind conditions by
14 coupling the unstructured-mesh hydrodynamic model SLIM with the
15 wave model SWAN. We apply the coupled model in the Florida Reef
16 Tract during Hurricane Irma (Sep. 2017) and show that it successfully
17 reproduces both the observed wave behavior and storm surge during
18 the hurricane. The modeled currents were then used to simulate the
19 trajectories of passive drifters during the passage of the hurricane. Our
20 results show that taking wave force into account induces variations of
21 up 1 m/s in modelled currents on the continental shelf break as well
22 as in the vicinity of reefs and islands. Wave-current interactions can
23 therefore deflect the trajectories of drifting material by up to 10 km on
24 the passage of the storm **Add something?**. These results strongly advo-
25 cate for the inclusion of wave forces while studying transport processes
26 (sediments, pollutants, larvae, etc.) in heavy-wind conditions.

²⁷ **1 Introduction**

²⁸ Wave-current interactions in coastal areas are of great importance for coastal
²⁹ engineering as they play a key role in sediment transport, morphological
³⁰ evolution and pollutant mixing (Bever and MacWilliams, 2013; Li and Johns,
³¹ 1998). However, these interactions are highly nonlinear and can vary sig-
³² nificantly in space and time (Wu et al., 2011). Wave-induced currents are
³³ generated by wave radiation gradients (Longuet-Higgins, 1970), affecting
³⁴ water levels near shorelines and wave breaking points (Longuet-Higgins
³⁵ and Stewart, 1964), while changes in water levels and currents, in turn,
³⁶ affect the motion and evolution of the waves (Sikirić et al., 2013). Cou-
³⁷ pled wave-current models are therefore required to capture these complex
³⁸ interactions.

³⁹ As coastal oceans are characterized by complex topology with islands,
⁴⁰ inlets and estuaries, unstructured (usually two-dimensional) models are pre-
⁴¹ ferred as structured grid models show limitations in resolving topologically-
⁴² controlled nearshore processes (Wu et al., 2011; Chen et al., 2007). The
⁴³ effect of wave-interactions becomes even more significant in the case of
⁴⁴ hurricanes, that generate large wind-waves and disturb ocean conditions
⁴⁵ (Liu et al., 2020) by causing coastal upwellings on continental shelves
⁴⁶ (Smith, 1982) and inducing strong currents, waves and storm surges in
⁴⁷ nearshore and coastal regions (Dietrich et al., 2010; Weisberg and Zheng,
⁴⁸ 2006). South Florida and the Gulf of Mexico are particularly vulnerable to
⁴⁹ hurricanes (Malmstadt et al., 2009) and modelling studies predict tropical
⁵⁰ cyclones to increase both in frequency and intensity in this region (Mar-
⁵¹ sooli et al., 2019; Knutson et al., 2010). Being able to accurately model
⁵² wave-current interactions in this area becomes thus critical.

⁵³ Individual-based modelling of particulates has been extensively used to
⁵⁴ study the transport of drifting materials such as pollutants, sediments or
⁵⁵ larvae (Garcia-Pineda et al., 2020; Liubartseva et al., 2018; Figueiredo et al.,
⁵⁶ 2013; Frys et al., 2020). Although some of these studies take the impact
⁵⁷ of waves into account by adding a Stokes drift velocity, *i.e.* the net drift of a
⁵⁸ floating particle in the direction of the wave propagation (Van Den Bremer
⁵⁹ and Breivik, 2018), to the Eulerian currents, they usually neglect the wave-
⁶⁰ induced currents. Such practice is reasonable in the case of fair weather,

61 when wave-induced forces exerted on currents are relatively smaller, but
62 might lead to significant inaccuracies during storm conditions. To assess
63 the importance of wave-current interactions during a tropical cyclone, we
64 investigated the transport of drifting particulates on the Florida shelf during
65 Hurricane Irma, one of the strongest and costliest tropical cyclones on
66 records in the Atlantic Basin (Chen et al., 2007), that made landfall in Florida
67 in September 2017.

68 In this study, we developed an unstructured coupled wave-current model of
69 South Florida to simulate the ocean circulation during hurricane Irma. Both
70 modelled currents and waves were validated against field measurements
71 and were then used to simulate the transport of drifting material in the
72 Florida Keys and the Florida inner shelf during the storm. Model outputs
73 were then compared with uncoupled simulation results in order to assess
74 the impact of wave-induced forces and Stokes drift on the modelled currents
75 and transports.

76 **2 Methods**

77 **2.1 Study area and observational data**

78 Large-scale ocean circulation around South Florida is dominated by the
79 Florida Current (FC), which originates from the Loop Currents (LC) where it
80 enters the Florida Straits from the Gulf of Mexico, and, downstream, forms
81 the Gulf Stream. The FC is a major western boundary current character-
82 ized by spatial variability and meandering, associated with the presence
83 of cyclonic eddies between the core of the current and the complex reef
84 topography of the Florida Reef Tract (FRT) (Lee et al., 1995; Kourafalou and
85 Kang, 2012). The northern half of these reefs are made of early Holocene
86 reef frameworks and indurated sand ridges while the southern part (the
87 Florida Keys) is composed of a chain of limestone islands, fossilized rem-
88 nants of ancient coral reefs and sand bars (Hoffmeister and Multer, 1968;
89 Shinn, 1988; Lidz and Shinn, 1991). The variability of the FC extends over
90 a large range of spatial and temporal scales, with periods of 30-70 days in
91 the Lower Keys (Lee et al., 1995) and shorter periods of 2-21 days in the
92 Upper Keys (Lee and Mayer, 1977), and exhibits significant seasonal and

93 interannual cycles (Johns and Schott, 1987; Lee and Williams, 1988; Schott
94 et al., 1988). Circulation on the West Florida Shelf (WFS) on the other hand
95 is forced by local winds and tidal fluctuations (Lee and Smith, 2002; Liu and
96 Weisberg, 2012).

97 The state of the ocean around Florida is monitored by an extensive array
98 of tide gauges, current meters and buoys. In this study, we used sea
99 surface elevation measurements from the National Oceanic and Atmospheric
100 Administrations (NOAA) Tides and Currents dataset. These measurements
101 were taken at four locations: two in the Florida Keys (Key West and Vaca
102 Key); one on the eastern coast of Florida (Key West); and one on the western
103 coast (Naples). For the currents, we used ADCP measurements from
104 the University of South Florida's College of Marine Science's (USF/CMS)
105 Coastal Ocean Monitoring and Prediction System (COMPS) for the WFS
106 (Weisberg et al., 2009). More specifically, we used measurements from
107 moorings C10, C12 and C13, respectively located at the 25, 50, and 50
108 m isobaths of the WFS (Liu et al., 2020). Finally, for the waves, we used
109 measurements from four buoys of the NOAA's National Data Buoy Center
110 (NDBC). Two on Florida's Eastern shelf and two on the WFS. The locations
111 of all measurement stations are shown on Fig. 1

112 **2.2 Wind and atmospheric pressure during Hurricane Irma**

113 Irma made landfall in Florida on 10 September 2017 as a category 3 storm,
114 first at Cudjoe Key (Florida Keys) and later on Marco Island, south to Naples
115 (see hurricane track in Fig. 1). It then weakened to a category 2 storm as it
116 moved further inland (Pinelli et al., 2018). The storm caused damages to
117 up to 75% of the buildings at his landfall point in the Florida Keys, making it
118 one of the strongest and costliest hurricanes on record in the Atlantic basin
119 (Xian et al., 2018; Zhang et al., 2019). The strongest reported wind speed
120 was 50 m/s on Marco Island while the highest recorded storm surge was
121 2.3 m, although larger wind speed likely occurred in the Florida Keys (Pinelli
122 et al., 2018) In order to reproduce the wind profile of Irma in our model,
123 we used high-resolution H*Wind wind fields (Powell et al., 1998). As these
124 data represent 1-min averaged wind speeds, we multiplied them by a factor
125 0.93 to obtain 10-min averaged wind speeds (Harper et al., 2010), which

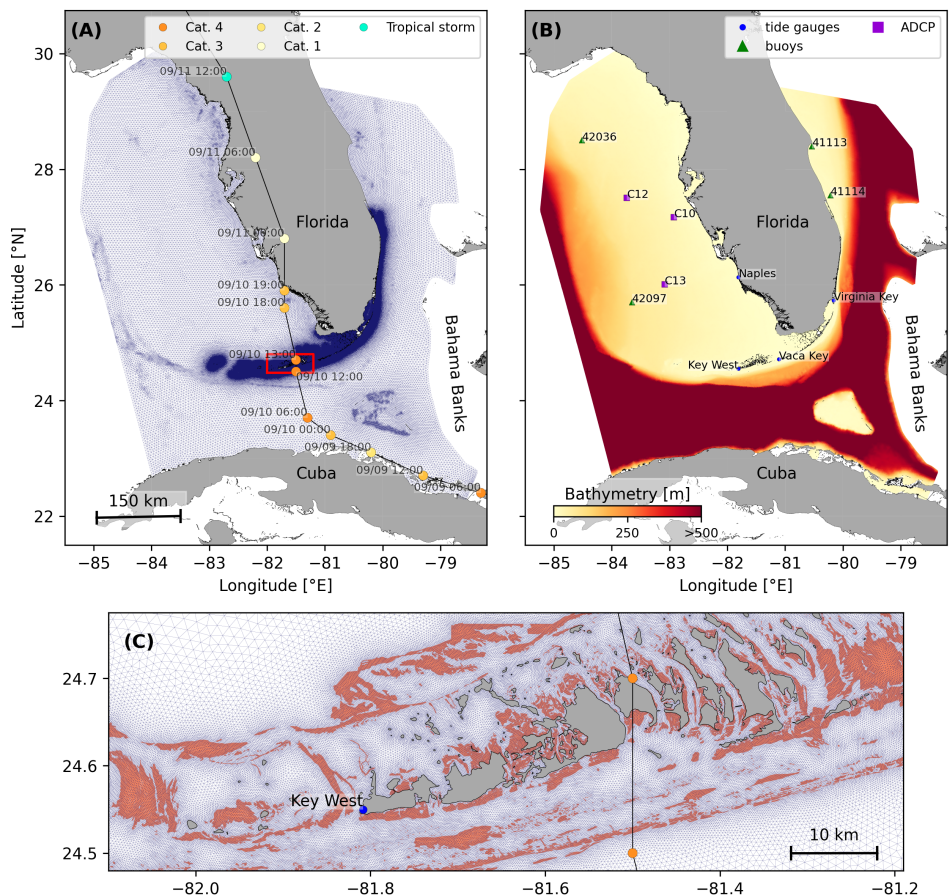


Fig. 1: **(A)** Mesh of the computational domain with the trajectory of Irma, category of the hurricane is given by the Saffir-Simpson color scale. **(B)** Bathymetry of the domain with the location of stations used for the validation of the model outputs. **(C)** Close up view of the Lower Keys area, where the mesh resolution reaches 100m near reefs (shown in coral) and islands (highlighted in dark grey)

126 are more consistent with the time step of our model. Furthermore, H*Wind
 127 wind profiles did not cover the whole model extent during the hurricane and
 128 were thus blended within coarser wind field extracted from ECMWF ERA-5
 129 datasets. Pressure fields of Irma were also constructed using ERA-5 data.
 130 However, the coarse resolution of the data set caused the depression at the
 131 center of the hurricane to get smoothed out, leading to an underestimation of
 132 the pressure gradient in our model. To better capture the central depression
 133 of Irma, we built a hybrid pressure field using the position and the minimal
 134 pressure of the core of the hurricane based on its track as recorded in
 135 the HURDAT 2 database (Landsea and Franklin, 2013). Based on this
 136 information, the hybrid pressure field was constructed by combining an
 137 idealized Holland pressure profile (Lin and Chavas, 2012) within the radius
 138 of maximum wind speed of Irma (Knaff et al., 2018) with ERA-5 pressure
 139 field. The transition between from the Holland profile to ERA-5 data outside
 140 the radius of maximum wind speed data was performed using a smooth step
 141 function.

142 **2.3 Hydrodynamic model**

143 Ocean currents generated during hurricane Irma around South Florida were
 144 modelled using the 2D barotropic version of the unstructured-mesh coastal
 145 ocean model SLIM¹. The model mesh covers an area similar to the model
 146 extent of Dobbelaere et al. (2020b), that includes the FRT but also the Florida
 147 Strait and part of the Gulf of Mexico (Figure 1). However, this area has
 148 been slightly extended northeastward and westward in order to include the
 149 NOAA-NDBC buoys. Furthermore, in order to withstand potential cell drying
 150 during the hurricane, we solved the conservative shallow water equations
 151 with wetting-drying:

$$\begin{aligned}
 \frac{\partial H}{\partial t} + \nabla \cdot (\mathbf{U}) &= 0, \\
 \frac{\partial \mathbf{U}}{\partial t} + \nabla \cdot \left(\frac{\mathbf{U}\mathbf{U}}{H} \right) &= -f \mathbf{e}_z \times \mathbf{U} + \alpha g H \nabla(H - h) - \frac{1}{\rho} \nabla p_{\text{atm}} + \frac{1}{\rho} \boldsymbol{\tau}_s \quad (1) \\
 &\quad + \nabla \cdot (\nu \nabla \mathbf{U}) - \frac{C_b}{H^2} |\mathbf{U}| \mathbf{U} + \gamma (\mathbf{U}_* - \mathbf{U}),
 \end{aligned}$$

¹<https://www.slim-ocean.be>

152 where H is the water column height and \mathbf{U} is the depth-averaged transport;
 153 f is the Coriolis coefficient; g is the gravitational acceleration; h is the
 154 bathymetry; α is a coefficient stating whether the mesh element is wet
 155 ($\alpha = 1$) or dry ($\alpha = 0$); ν is the viscosity; C_b is the bulk bottom drag
 156 coefficient; ∇p_{atm} is the atmospheric pressure gradient; τ_s is the surface
 157 stress due to wind; and γ is a relaxation coefficient towards a reference
 158 transport \mathbf{U}_* . As in Frys et al. (2020) and Dobbelaere et al. (2020b), SLIM
 159 currents were gradually relaxed towards HYCOM (Chassignet et al., 2007) in
 160 regions where the water depth exceeds 50m.

161 At very high wind speeds, the white cap is blown off the crest of the waves,
 162 which generates a layer of droplets that acts as a slip layer for the winds
 163 at the ocean-atmosphere interface (Holthuijsen et al., 2012). This causes
 164 a saturation of the wind drag coefficient for strong winds (Donelan et al.,
 165 2004; Powell et al., 2003). To account for the impact of this saturation
 166 on the surface wind stress in our model, we implemented the wind drag
 167 parameterization of Moon et al. (2007). In this parameterization, the drag
 168 coefficient C_d depends on the wind speed at 10-m height U_{10} according to:

$$C_d = \kappa^2 \log \left(\frac{10}{z_0} \right)^{-2} \quad (2)$$

169 where κ is the von Karman constant. The roughness length z_0 in Eq. (2) is
 170 expressed as:

$$z_0 = \begin{cases} \frac{0.0185}{g} U_*^2 & \text{if } U_{10} \leq 12.5 \text{ m/s ,} \\ [0.085(-0.56U_*^2 + 20.255U_* + 2.458) - 0.58] \times 10^{-3} & \text{if } U_{10} > 12.5 \text{ m/s ,} \end{cases} \quad (3)$$

171 with U_* the friction velocity. The relation between U_{10} and U_* is given by:

$$U_{10} = -0.56U_*^2 + 20.255U_* + 2.458 . \quad (4)$$

172 The mesh resolution depends on the distance to coastlines and reefs follow-
 173 ing the approach of (Dobbelaere et al., 2020b). The mesh was then further
 174 refined as a function of bathymetry and bathymetry gradient, as suggested

175 by SWAN documentation². Such approach improves the efficiency of the
 176 computational grid by locally increasing the mesh resolution in areas where
 177 the bathymetry or evolution of the waves change rapidly while avoiding to
 178 invest too many computational resources where the physics or depth change
 179 less. The mesh was generated using the Python library seamsh³, based
 180 on the open-source mesh generator GMSH (Geuzaine and Remacle,
 181 2009). It is composed of approximately 7.7×10^5 elements. The coarsest
 182 elements, far away from the FRT, had a characteristic length size of about 5
 183 km whereas the finest elements had a characteristic length of 100 m near
 184 coastlines and reefs (Fig 1).

185 **2.4 Wave model**

186 Waves were modelled using the parallel unstructured-mesh version of the
 187 Simulating WAves Nearshore (SWAN) model (Booij et al., 1999), one of the
 188 most commonly used wave models in coastal areas and inland waters. This
 189 model solves the action balance equation, which reads (Mei, 1989):

$$\frac{\partial N}{\partial t} + \nabla_x \cdot [(c_g + \mathbf{u})N] + \frac{\partial}{\partial \theta}[c_\theta N] + \frac{\partial}{\partial \sigma}[c_\sigma N] = \frac{S_{in} + S_{ds} + S_{nl}}{\sigma}, \quad (5)$$

190 where $N = E/\sigma$ is the wave action density; θ is the wave propagation
 191 direction; σ is the wave relative frequency; c_g is the wave group velocity,
 192 $\mathbf{u} = \mathbf{U}/H$ is SLIM depth-averaged current velocity; c_θ and c_σ are the propa-
 193 gation velocities in spectral space due to refraction and shifting in frequency
 194 due to variations in depth and currents; and S_{in} , S_{ds} , and S_{nl} respectively
 195 represent wave growth by wind, wave decay and nonlinear transfers of
 196 wave energy through interactions between triplets and quadruplets. Spectra
 197 were discretized with 48 direction bins and 50 frequency bins logarithmically
 198 distributed from 0.3 to 2 Hz. Exponential wind growth was parameterized
 199 using the formulation of Janssen (1991), while dissipations by whitecapping
 200 and bottom dissipations followed the formulations of Komen et al. (1984)
 201 and Madsen et al. (1989) respectively. Coefficients for exponential wind
 202 growth and whitecapping parameterizations were based on the results of
 203 Siadatmousavi et al. (2011), that significantly differ from SWAN's default

²<http://swanmodel.sourceforge.net/unswan/unswan.htm>

³<https://pypi.org/project/seamsh/>

204 settings. Formulation of Komen et al. (1984) is used by default by SWAN
 205 for wind energy input while default parameters for whitecapping [wait for
 206 zenobe to be back]. The choice of these formulations was motivated by
 207 the appearance of numerical instabilities in the region of the Gulf Stream
 208 using SWAN's default parameter values. Finally, wave boundary conditions
 209 were derived from WAVEWATCH III (Tolman et al., 2009) spectral outputs at
 210 buoy locations. Surface wave induce a net drift in te direction of the wave
 211 propagation, known as Stokes drift (Van Den Bremer and Breivik, 2018;
 212 Stokes, 1880). This net drift has significant impacts on sediment motion
 213 in near shore regions (Hoefel and Elgar, 2003), the formation of Langmuir
 214 cells (Langmuir, 1938; Craik and Leibovich, 1976) as well as the transport of
 215 heat, salt or pollutants such as oil or micro-plastic in the upper ocean layer
 216 (McWilliams and Sullivan, 2000; Röhrs et al., 2012; Drivedal et al., 2014).
 217 To model adequately the Stokes profile in mixed wind-driven sea and swell
 218 conditions, the full two- dimensional wave spectrum must be represented
 219 by a spectral wave model within a wave-current coupling (Van Den Bremer
 220 and Breivik, 2018). In this study, depth-averaged Stokes drift was therefore
 221 computed by SWAN using the following formula:

$$\mathbf{u}_s = \int_0^{2\pi} \int_0^{+\infty} \frac{\sigma^3}{h \tanh(2kh)} E(\sigma, \theta) (\cos \theta, \sin \theta) d\sigma d\theta, \quad (6)$$

222 where k is the norm of the wave vector; h is the water depth; and $E(\sigma, \theta)$ is
 223 the wave energy density.

224 2.5 Coupled model

225 SLIM and SWAN are coupled so that they run on the same computational
 226 core and the same unstructured mesh. SLIM is run first and passes com-
 227 puted wind velocities (\mathbf{U}_{10}), water levels ($\eta = H - h$) and depth-averaged
 228 currents ($\mathbf{u} = \mathbf{U}/H$) to SWAN, as well as a roughness length (z_0) for the bot-
 229 tom dissipation formulation of Madsen et al. (1989). This roughness length
 230 is computed from SLIM's bulk drag coefficient C_b following the approach of
 231 Dietrich et al. (2011) so that both models have consistent bottom dissipation
 232 parameterizations. SWAN then utilizes these quantities to compute the wave
 233 radiation stress gradient, that is then passed to SLIM as the wave-induced
 234 stress on currents τ_{wave} . SLIM then uses this quantity to update the the

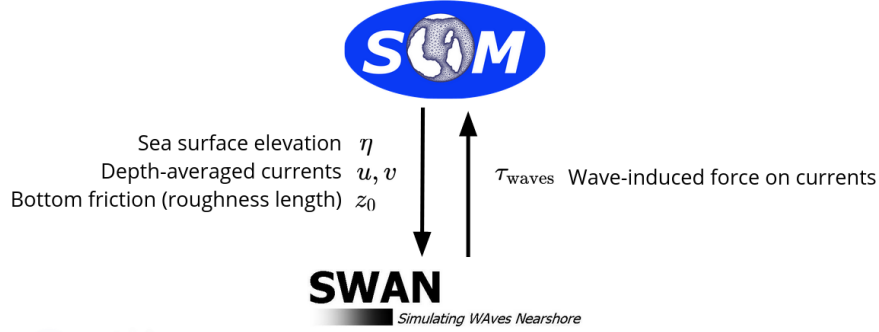


Fig. 2: Schematic illustration of the coupled SLIM+SWAN model.

235 value of the surface stress τ_s in Eq. (1), that now becomes the sum of wind
 236 and wave-induced stresses $\tau_s = \tau_{\text{wind}} + \tau_{\text{wave}}$.

237 SLIM equations are integrated using an implicit scheme while SWAN is
 238 unconditionally stable (Dietrich et al., 2010), allowing both models to be run
 239 with relatively large time steps. In this study, both models were therefore
 240 run sequentially using a time step of 600s, so that each computational core
 241 was alternating running either SLIM or SWAN. As in the coupling between
 242 SWAN and ADCIRC (Dietrich et al., 2010), both models utilize the same
 243 local sub-mesh, allowing for a one-to-one correspondence between the
 244 geographic locations of the mesh vertices. No interpolation is therefore
 245 needed when passing computed quantities from a model to another, which
 246 allows for efficient inter-model communication. However, as SLIM applies
 247 discontinuous Galerkin finite element methods, an additional conversion step
 248 to a continuous framework was required to transmit SLIM nodal quantities to
 249 SWAN.

250 3 Results

251 We first validated the reconstructed atmospheric fields of hurricane Irma as
 252 well the modelled currents and waves of our coupled model against fields
 253 measurements. Once we had built some confidence in our model accuracy
 254 we used these, we used these modelled quantities to represent the transport
 255 of passive particles in the Lower Florida Keys during the passage of the
 256 hurricane. These transports were obtained using three data sets: (i) currents

257 from an uncoupled SLIM simulation of Irma (SLIM); (ii) currents modelled
258 by the coupled SLIM+SWAN model (SLIM+SWAN); (iii) currents modelled
259 by the coupled SLIM+SWAN model to which the modelled depth-averaged
260 Stokes drift was added (Eq. 6) (SLIM+SWAN+Stokes). We then compared
261 the particle trajectories obtained with these three sets of currents to assess
262 the impact of wave-current coupling on drifter transport during the passage
263 of a major hurricane.

264 **3.1 Model validation**

265 H*Wind winds and hybrid pressure field agree well with station measure-
266 ments at Vaca Key station (Fig. 3). The hybrid pressure field shows better
267 agreement with observations than ERA-5 pressure as it successfully re-
268 produces the storm depression. ERA-5 fields, on the other hand, fail to
269 resolve the low pressure at the core of the hurricane due to their coarser
270 grid, leading to an overestimation of 8 mbar of the storm depression. Both
271 H*Wind and ERA-5 agree well with observed wind speeds although both
272 data sets tend to slightly overestimate the width and intensity of the wind
273 peak. However, H*wind profiles show a better match with the timing of the
274 observed peak, as ERA-5 winds tend to anticipate it. H*wind also exhibits a
275 slightly narrower peak in wind speed, which better agrees with observations.

276 Hydrodynamic outputs of the coupled wave-current agree well with tide
277 gauge (Fig. 4) and ADCP measurements (Fig. 5). The timing and amplitude
278 of the storm surges are well reproduced by the coupled model, the largest
279 model error being an overestimation of 18 cm of the elevation peak at
280 Virginia Key. The fit is especially good at Naples, where both the positive
281 and negative surges are captured by the coupled model with an error of less
282 than 5 cm. This result is of interest as negative surges, although less studied,
283 affect water exchanges between the estuaries and the coastal ocean and
284 disturb the benthic ecosystems (Liu et al., 2020). Modelled 2D currents were
285 validated against depth-averaged ADCP measurements at mooring station
286 C10, C12 and C13 (Fig. 5). As in Liu et al. (2020), the vector correlation
287 analysis of Kundu (1976) is performed to compare modelled and observed
288 current velocity vectors. Correlation coefficients (ρ) between simulated
289 and observed depth-averaged currents were 0.84, 0.74 and 0.73 at the

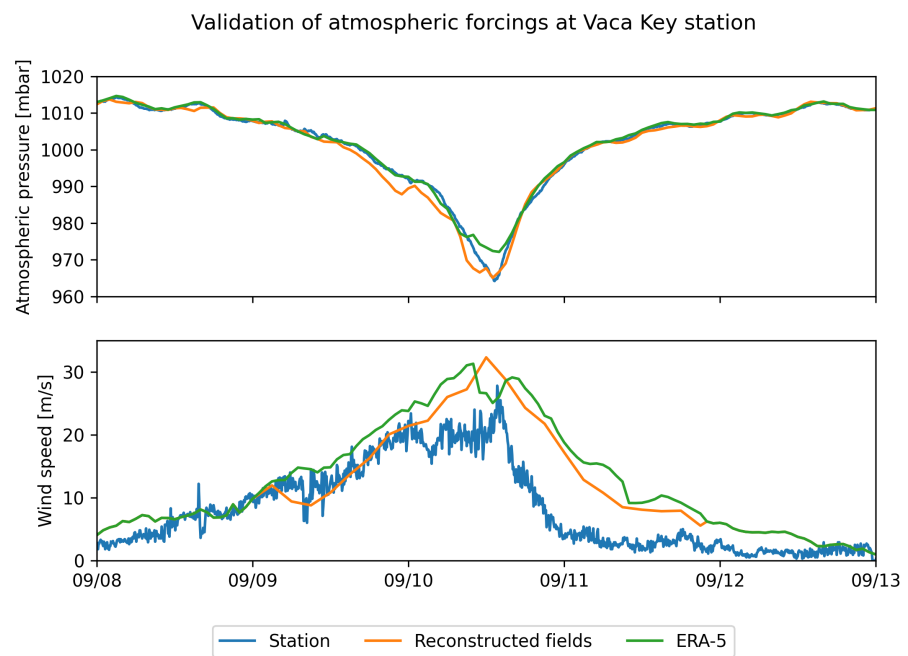


Fig. 3: Comparison of reconstructed wind atmospheric pressure with field measurements and coarser ECMWF ERA-5 profiles at Vaca Key station. The generated hybrid atmospheric forcings better capture the observed storm depression while H*wind winds better match the measured peak in wind speed.

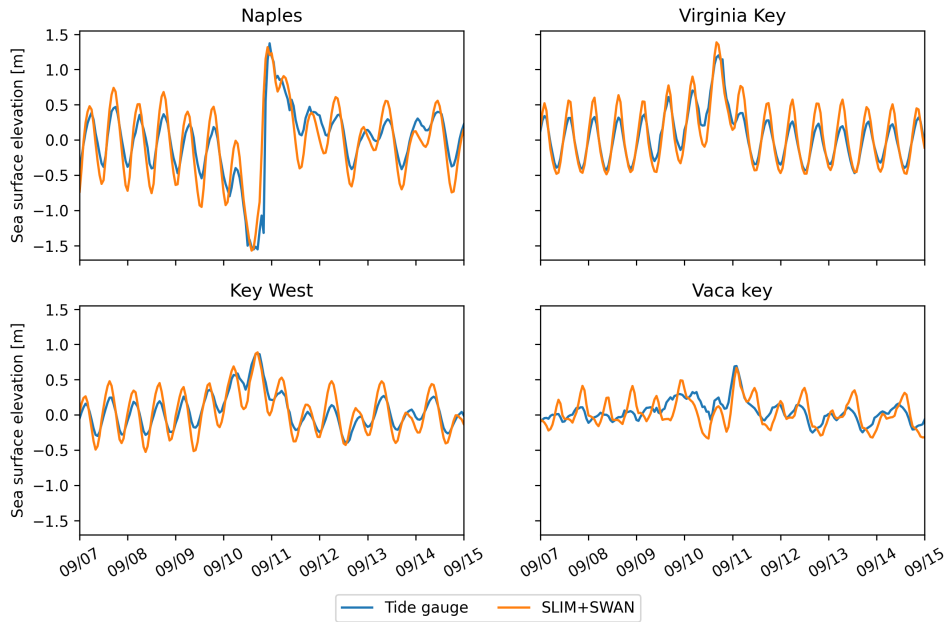


Fig. 4: Comparison of modelled sea surface elevation with all 4 tide gauge measurements (see Fig. 1B for their location). Timing and amplitudes of the storm surges are well reproduced by the model

C10, C12 and C13 locations, respectively. Average veering angles were computed as well and were below 12° , as in (Liu et al., 2020). However, in our case, no clear tendency regarding modelled current behavior compared to observations was observed. As expected from a depth-averaged model, the best fit with observations is obtained at the shallowest mooring C10, located on the 25m isobath, with an average veering angle of 6° .

The simulated significant wave height agrees well with observations on the WFS, where errors on the peak value do not exceed 5%. On the East Florida Shelf, errors are slightly larger reaching 20%. Although the model outputs agree well with observations, a lag in significant wave height is observed for all 4 buoys. Moreover, the peak in significant wave height tends to be underestimated at buoys 41113 and 41114, located on the East Florida Shelf. Other wave parameters were better reproduced by the model on the WFS as well, as illustrated for buoy 42036 in Fig. 6. This good fit on the WFS is not surprising as the parameters used for wind energy input and whitecapping dissipation were based on the calibration performed by (Siadatmousavi et al., 2011) on the Northern Gulf of Mexico. Wind-induced wave growth might

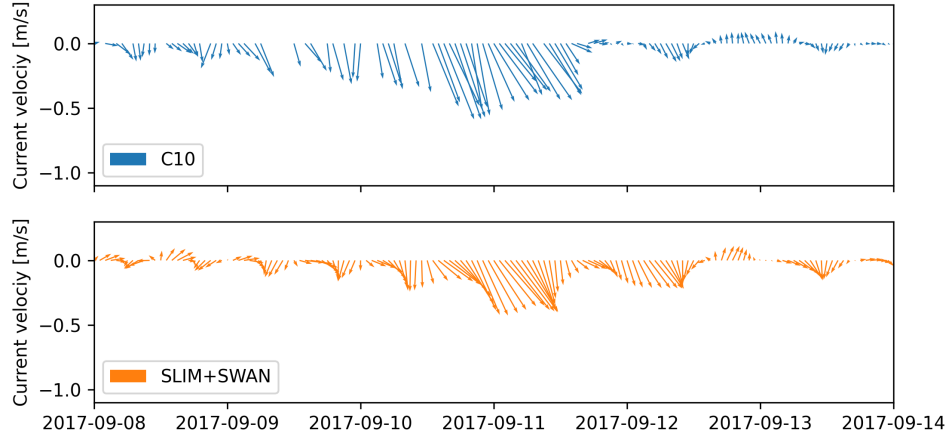


Fig. 5: Comparison of modelled current velocity with observed velocity at mooring C10 (see Fig. 1B for its location). Modelled current velocities agree well with observations, with a correlation coefficient of 0.83 and an average veering angle of 6° .

307 therefore be underestimated on the eastern shelf. Consequently, incident
 308 wave do not receive enough energy to grow after breaking on the bank
 309 boundary, leading to an underestimation of the significant wave height at
 310 the location of the buoys. Nonetheless, as this study focused on the wave
 311 produced by Irma, that made landfall on the western coasts of Florida, the
 312 use of parameterizations calibrated for the Gulf of Mexico seems reasonable.

313 3.2 Impact of waves on currents and transport

314 The impact of hurricane-induced wave-current interactions is first evaluated
 315 by computing the norm of the maximum difference in current velocity be-
 316 tween uncoupled SLIM and coupled SLIM+SWAN model runs during the
 317 passage of Irma through the Florida Keys (from 2017-09-07 to 2017-09-13).
 318 The differences in modelled currents appear to be stronger on the shelf
 319 break and over coral reefs (Fig. 7). These results highlight the significant
 320 impact of wave-induced forces, that can yield differences of up to 1 m/s dur-
 321 ing the hurricane, with stronger currents being obtained with SLIM+SWAN.
 322 This suggests that neglecting wave-current interactions during Irma would
 323 results in a significant underestimation of transport over reefs.

324 To quantify the impact of these differences in velocity fields, we compared

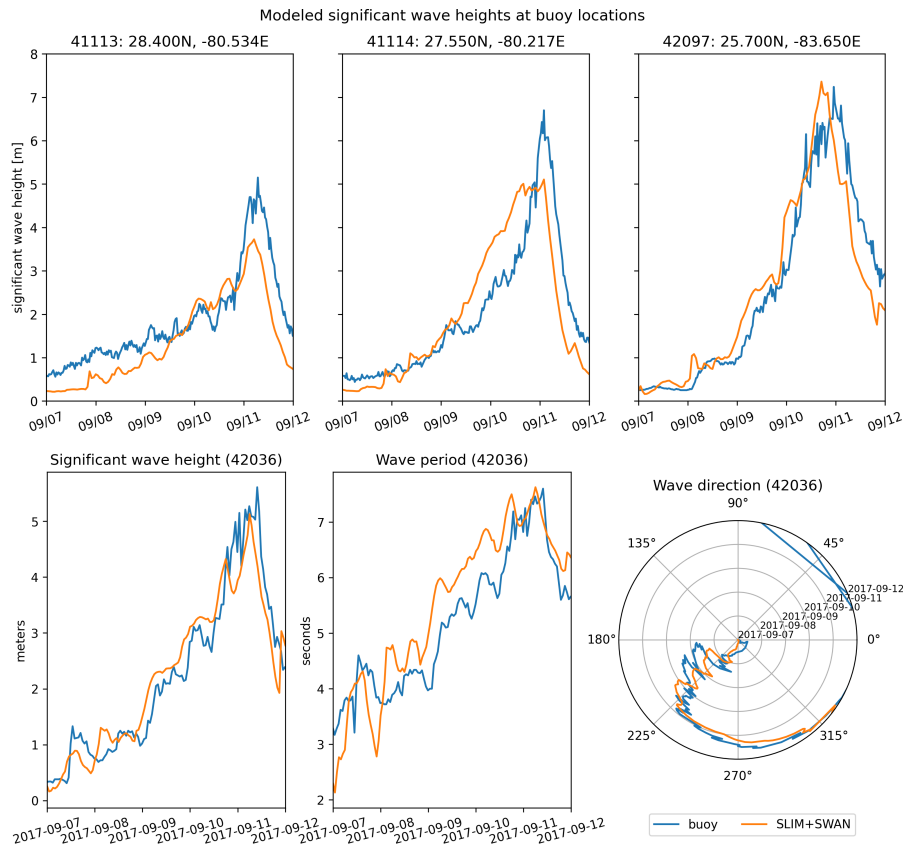


Fig. 6: Comparison of modelled wave parameters with observation at the 4 buoys location (locations shown in Fig. 1B). Modelled significant wave height agrees well with field measurement. As model parameters were calibrated for the Northern Gulf of Mexico, observations are better reproduced at buoys located on the WFS, as illustrated for buoy 42036

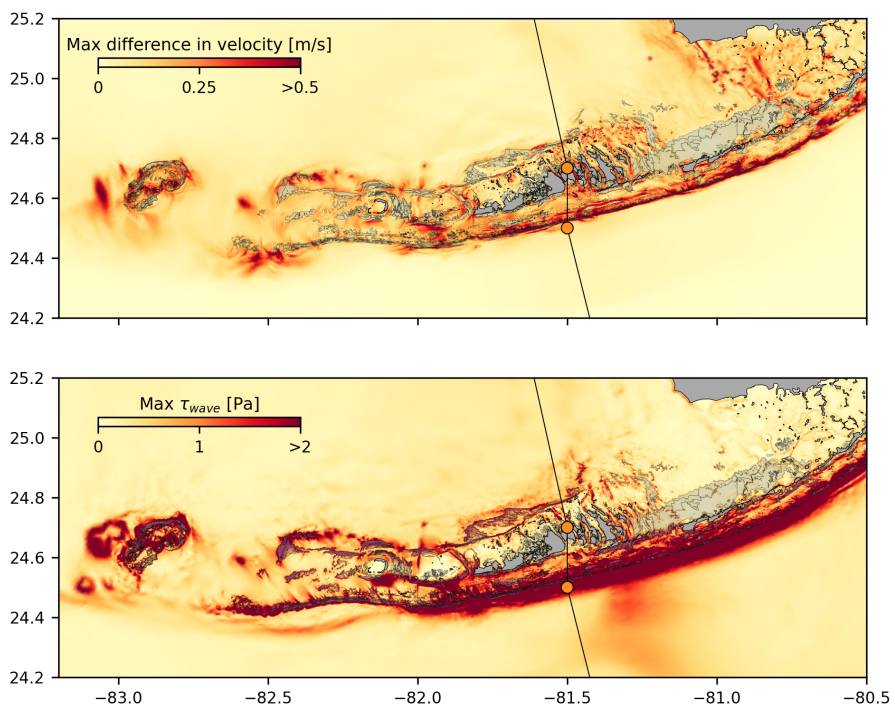


Fig. 7: Maximum of the difference between SLIM and SLIM+SWAN currents speed between 2017-09-07 00:00:00 and 2017-09-13 00:00:00. The difference between the coupled and uncoupled model, which represents the effect of the wave-induced stress, can yield differences of 0.5 m/s in the simulated currents during the passage of the hurricane. SLIM+SWAN currents velocities are larger than the currents modeled by SLIM alone. Islands are highlighted in dark grey and coral reefs in lighter grey

325 the trajectories of virtual particles driven by currents produced by SLIM
326 alone and SLIM+SWAN simulations in the Florida Keys. First, we identified
327 the areas where the differences between the modelled currents were the
328 largest. Then, we determined the potential origination regions of particles
329 reaching these areas on the passage of the hurricane through the Florida
330 Keys using backtracking methods (Dobbelaeere et al., 2020a). These regions
331 are highlighted by the 4 release regions of Fig. 8. Finally, particles were
332 released from these four regions and advected by currents produced by the
333 coupled and uncoupled models. At each time step, the center of mass of
334 the modelled particle clouds were computed. The distance between these
335 centers of mass was used as a measure of the impact of the wind-generated
336 wave coupling on the modelled current in the Florida Keys during hurricane
337 Irma. This comparison was performed with 3 sets of currents: the currents
338 modelled by uncoupled SLIM (SLIM); the currents modelled by coupled
339 SLIM+SWAN (SLIM+SWAN); and the SLIM+SWAN currents with depth-
340 averaged Stokes drift (SLIM+SWAN+Stokes) [sentence is too condensed].
341 The results of these comparisons are shown in Fig. 8 [reformulate as active
342 sentence]. Differences between the modelled trajectories are negligible
343 before the passage of the hurricanes in the Florida Keys. Then, distance
344 between the centers of mass of the particles abruptly increase to up to
345 tens of kilometers as Irma gets through the Keys to finally stabilize after
346 the passage of the hurricane. These results support the assumption that
347 wave-induced transport is negligible compared to advection by Eulerian
348 currents in fair weather conditions. Particles advected by the currents of
349 the coupled model tend to remain on the shelf while particles advected by
350 SLIM alone are mostly transported along the shelf break. Although not
351 shown in this paper, comparison of SLIM and SLIM+SWAN trajectories were
352 conducted as well. The evolution of the distance between centers of mass
353 of the particle clouds showed similar trends while yielding smaller values.
354 Modelled maximal depth-averaged Stokes drift reached up to 0.2 m/s during
355 the passage of Irma through the Florida Keys. This suggests that both the
356 impact of wave-induced force on Eulerian currents and Stokes drift should be
357 taken into account while modelling particle transport under storm conditions.

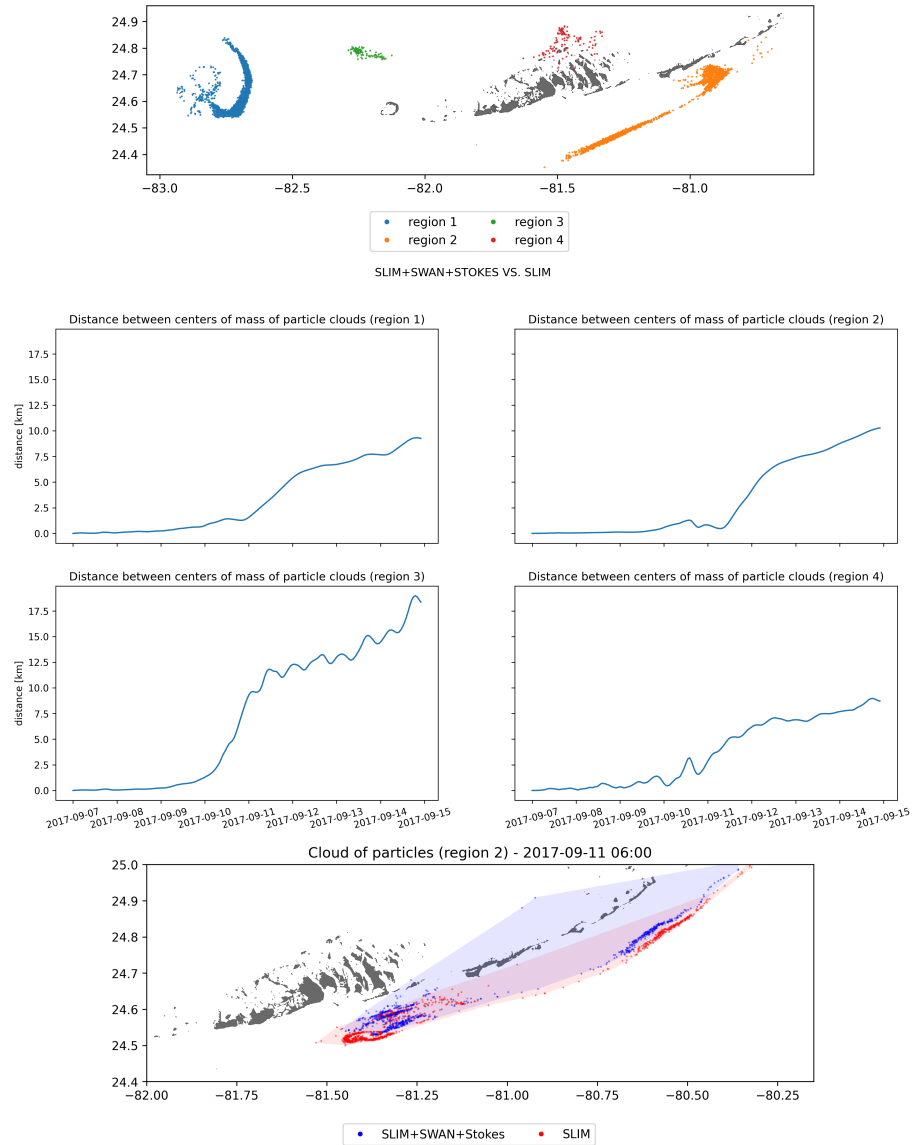


Fig. 8: Comparison of passive drifters trajectories with SLIM+SWAN+Stokes drift vs. SLIM alone. A snapshot of the positions of the particles released from region 2 is shown after the passage of Irma in the Florida Keys. Particles advected by the currents of the coupled model tend to remain on the shelf while particles advected by SLIM alone are mostly transported along the shelf break

358 4 Discussion and conclusions

359 Impact of waves on coral connectivity

360 Ability of wave model to correctly capture gradient in significant wave height
361 due to current-waves interactions under tropical cyclones depends on:

362 • Broad perspective \Rightarrow not limited to FL

363 • Mention search and rescue

364 • However, ignoring waves in storm conditions could result in significant
365 inaccuracies in modelled trajectories, as illustrated in the case of
366 release region 2 in Fig. 8

367 • Spatial (10km \rightarrow 5km) and spectral (36 dir. \rightarrow 48 dir.) resolution
368 (Hegermiller et al., 2019)

369 • Directional spreading of incident waves (Villas Bôas et al., 2020)

370 Conflict of Interest Statement

371 The authors declare that the research was conducted in the absence of any
372 commercial or financial relationships that could be construed as a potential
373 conflict of interest.

374 Author Contributions

375 Funding

376 Acknowledgments

377 Computational resources were provided by the Consortium des Équipements
378 de Calcul Intensif (CÉCI), funded by the F.R.S.-FNRS under Grant No. 2.5020.11.
379 Thomas Dobbelaere is a PhD student supported by the Fund for Research
380 training in Industry and Agriculture (FRIA/FNRS).

381 Supplementary Material

382The Supplementary Material for this article is attached to the submitted
383document.

384 References

- 385**Bever, A. J. and MacWilliams, M. L. (2013). Simulating sediment transport
386processes in San Pablo Bay using coupled hydrodynamic, wave, and
387sediment transport models. *Marine Geology*, 345:235–253.
- 388**Booij, N., Ris, R. C., and Holthuijsen, L. H. (1999). A third-generation wave
389model for coastal regions: 1. Model description and validation. *Journal*
390of *geophysical research: Oceans*, 104(C4):7649–7666.
- 391**Chassignet, E. P., Hurlbert, H. E., Smedstad, O. M., Halliwell, G. R., Hogan,
392P. J., Wallcraft, A. J., Baraille, R., and Bleck, R. (2007). The HYCOM
393(hybrid coordinate ocean model) data assimilative system. *Journal of*
394*Marine Systems*, 65(1-4):60–83.
- 395**Chen, C., Huang, H., Beardsley, R. C., Liu, H., Xu, Q., and Cowles, G. (2007).
396A finite volume numerical approach for coastal ocean circulation studies:
397Comparisons with finite difference models. *Journal of Geophysical*
398*Research: Oceans*, 112(C3).
- 399**Craik, A. D. and Leibovich, S. (1976). A rational model for Langmuir circula-
400tions. *Journal of Fluid Mechanics*, 73(3):401–426.
- 401**Dietrich, J., Bunya, S., Westerink, J., Ebersole, B., Smith, J., Atkinson,
402J., Jensen, R., Resio, D., Luettich, R., Dawson, C., et al. (2010). A
403high-resolution coupled riverine flow, tide, wind, wind wave, and storm
404surge model for southern Louisiana and Mississippi. part ii: Synoptic
405description and analysis of hurricanes Katrina and Rita. *Monthly Weather*
406*Review*, 138(2):378–404.
- 407**Dietrich, J., Westerink, J., Kennedy, A., Smith, J., Jensen, R., Zijlema, M.,
408Holthuijsen, L., Dawson, C., Luettich, R., Powell, M., et al. (2011).
409Hurricane Gustav (2008) waves and storm surge: Hindcast, synoptic

- 410 analysis, and validation in southern Louisiana. *Monthly Weather Review*,
411 139(8):2488–2522.
- 412 Dobbelaere, T., Muller, E., Gramer, L., Holstein, D., and Hanert, E. (2020a).
413 Report on the potential origin of the SCTLD in the Florida Reef Tract.
414 Available online at: [https://floridadep.gov/rcp/coral/documents/
415 report-potential-origin-sctld-florida-reef-tract](https://floridadep.gov/rcp/coral/documents/report-potential-origin-sctld-florida-reef-tract).
- 416 Dobbelaere, T., Muller, E. M., Gramer, L. J., Holstein, D. M., and Hanert, E.
417 (2020b). Coupled epidemic-hydrodynamic modeling to understand the
418 spread of a deadly coral disease in Florida. *Frontiers in Marine Science*,
419 7:1016.
- 420 Donelan, M., Haus, B., Reul, N., Plant, W., Stiassnie, M., Gruber, H., Brown,
421 O., and Saltzman, E. (2004). On the limiting aerodynamic roughness of
422 the ocean in very strong winds. *Geophysical Research Letters*, 31(18).
- 423 Drivdal, M., Broström, G., and Christensen, K. (2014). Wave-induced mixing
424 and transport of buoyant particles: application to the statfjord a oil spill.
425 *Ocean Science*, 10(6):977–991.
- 426 Figueiredo, J., Baird, A. H., and Connolly, S. R. (2013). Synthesizing larval
427 competence dynamics and reef-scale retention reveals a high potential
428 for self-recruitment in corals. *Ecology*, 94(3):650–659.
- 429 Frys, C., Saint-Amand, A., Le Hénaff, M., Figueiredo, J., Kuba, A., Walker, B.,
430 Lambrechts, J., Vallaeyns, V., Vincent, D., and Hanert, E. (2020). Fine-
431 scale coral connectivity pathways in the Florida Reef Tract: implications
432 for conservation and restoration. *Frontiers in Marine Science*, 7:312.
- 433 Garcia-Pineda, O., Androulidakis, Y., Le Hénaff, M., Kourafalou, V., Hole,
434 L. R., Kang, H., Staples, G., Ramirez, E., and DiPinto, L. (2020). Mea-
435 suring oil residence time with GPS-drifters, satellites, and Unmanned
436 Aerial Systems (UAS). *Marine pollution bulletin*, 150:110644.
- 437 Geuzaine, C. and Remacle, J.-F. (2009). Gmsh: A 3-d finite element mesh
438 generator with built-in pre-and post-processing facilities. *International
439 journal for numerical methods in engineering*, 79(11):1309–1331.

- 440 Harper, B., Kepert, J., and Ginger, J. (2010). *Guidelines for converting*
441 *between various wind averaging periods in tropical cyclone conditions.*
442 Citeseer.
- 443 Hegermiller, C. A., Warner, J. C., Olabarrieta, M., and Sherwood, C. R.
444 (2019). Wave–current interaction between Hurricane Matthew wave
445 fields and the Gulf Stream. *Journal of Physical Oceanography*,
446 49(11):2883–2900.
- 447 Hoefel, F. and Elgar, S. (2003). Wave-induced sediment transport and
448 sandbar migration. *Science*, 299(5614):1885–1887.
- 449 Hoffmeister, J. and Multer, H. (1968). Geology and origin of the Florida Keys.
450 *Geological Society of America Bulletin*, 79(11):1487–1502.
- 451 Holthuijsen, L. H., Powell, M. D., and Pietrzak, J. D. (2012). Wind and waves
452 in extreme hurricanes. *Journal of Geophysical Research: Oceans*,
453 117(C9).
- 454 Janssen, P. A. (1991). Quasi-linear theory of wind-wave generation applied
455 to wave forecasting. *Journal of physical oceanography*, 21(11):1631–
456 1642.
- 457 Johns, W. E. and Schott, F. (1987). Meandering and transport variations
458 of the Florida Current. *Journal of physical oceanography*, 17(8):1128–
459 1147.
- 460 Knaff, J. A., Sampson, C. R., and Musgrave, K. D. (2018). Statistical tropi-
461 cal cyclone wind radii prediction using climatology and persistence:
462 Updates for the western North Pacific. *Weather and Forecasting*,
463 33(4):1093–1098.
- 464 Knutson, T. R., McBride, J. L., Chan, J., Emanuel, K., Holland, G., Landsea,
465 C., Held, I., Kossin, J. P., Srivastava, A., and Sugi, M. (2010). Tropical
466 cyclones and climate change. *Nature geoscience*, 3(3):157–163.
- 467 Komen, G., Hasselmann, S., and Hasselmann, K. (1984). On the exis-
468 tence of a fully developed wind-sea spectrum. *Journal of physical*
469 *oceanography*, 14(8):1271–1285.

- 470 Kourafalou, V. H. and Kang, H. (2012). Florida Current meandering and
471 evolution of cyclonic eddies along the Florida Keys Reef Tract: Are they
472 interconnected? *Journal of Geophysical Research: Oceans*, 117(C5).
- 473 Kundu, P. K. (1976). Ekman veering observed near the ocean bottom.
474 *Journal of Physical Oceanography*, 6(2):238–242.
- 475 Landsea, C. W. and Franklin, J. L. (2013). Atlantic hurricane database un-
476 certainty and presentation of a new database format. *Monthly Weather
477 Review*, 141(10):3576–3592.
- 478 Langmuir, I. (1938). Surface motion of water induced by wind. *Science*,
479 87(2250):119–123.
- 480 Lee, T. N., Leaman, K., Williams, E., Berger, T., and Atkinson, L. (1995).
481 Florida Current meanders and gyre formation in the southern Straits
482 of Florida. *Journal of Geophysical Research: Oceans*, 100(C5):8607–
483 8620.
- 484 Lee, T. N. and Mayer, D. A. (1977). Low-frequency current variability and
485 spin-off eddies along the shelf off southeast Florida. *Collected Reprints*,
486 1(1):344.
- 487 Lee, T. N. and Smith, N. (2002). Volume transport variability through the
488 Florida Keys tidal channels. *Continental Shelf Research*, 22(9):1361–
489 1377.
- 490 Lee, T. N. and Williams, E. (1988). Wind-forced transport fluctuations of the
491 Florida Current. *Journal of Physical Oceanography*, 18(7):937–946.
- 492 Li, Z. and Johns, B. (1998). A three-dimensional numerical model of surface
493 waves in the surf zone and longshore current generation over a plane
494 beach. *Estuarine, Coastal and Shelf Science*, 47(4):395–413.
- 495 Lidz, B. H. and Shinn, E. A. (1991). Paleoshorelines, reefs, and a rising sea:
496 South florida, usa. *Journal of Coastal Research*, pages 203–229.
- 497 Lin, N. and Chavas, D. (2012). On hurricane parametric wind and appli-
498 cations in storm surge modeling. *Journal of Geophysical Research:
499 Atmospheres*, 117(D9).

- 500 Liu, Y. and Weisberg, R. H. (2012). Seasonal variability on the West Florida
501 shelf. *Progress in Oceanography*, 104:80–98.
- 502 Liu, Y., Weisberg, R. H., and Zheng, L. (2020). Impacts of hurricane Irma
503 on the circulation and transport in Florida Bay and the Charlotte Harbor
504 estuary. *Estuaries and Coasts*, 43(5):1194–1216.
- 505 Liubartseva, S., Coppini, G., Lecci, R., and Clementi, E. (2018). Tracking
506 plastics in the Mediterranean: 2D Lagrangian model. *Marine pollution
507 bulletin*, 129(1):151–162.
- 508 Longuet-Higgins, M. S. (1970). Longshore currents generated by obliquely
509 incident sea waves. *Journal of geophysical research*, 75(33):6778–
510 6789.
- 511 Longuet-Higgins, M. S. and Stewart, R. (1964). Radiation stresses in water
512 waves; a physical discussion, with applications. In *Deep sea research
513 and oceanographic abstracts*, volume 11, pages 529–562. Elsevier.
- 514 Madsen, O. S., Poon, Y.-K., and Gruber, H. C. (1989). Spectral wave
515 attenuation by bottom friction: Theory. In *Coastal Engineering 1988*,
516 pages 492–504.
- 517 Malmstadt, J., Scheitlin, K., and Elsner, J. (2009). Florida hurricanes and
518 damage costs. *southeastern geographer*, 49(2):108–131.
- 519 Marsooli, R., Lin, N., Emanuel, K., and Feng, K. (2019). Climate change
520 exacerbates hurricane flood hazards along US Atlantic and Gulf Coasts
521 in spatially varying patterns. *Nature communications*, 10(1):1–9.
- 522 McWilliams, J. C. and Sullivan, P. P. (2000). Vertical mixing by Langmuir
523 circulations. *Spill Science & Technology Bulletin*, 6(3-4):225–237.
- 524 Mei, C. C. (1989). *The applied dynamics of ocean surface waves*, volume 1.
525 World scientific.
- 526 Moon, I.-J., Ginis, I., Hara, T., and Thomas, B. (2007). A physics-based
527 parameterization of air–sea momentum flux at high wind speeds and
528 its impact on hurricane intensity predictions. *Monthly weather review*,
529 135(8):2869–2878.

- 530 Pinelli, J.-P., Roueche, D., Kijewski-Correa, T., Plaz, F., Prevatt, D., Zisis,
531 I., Elawady, A., Haan, F., Pei, S., Gurley, K., et al. (2018). Overview
532 of damage observed in regional construction during the passage of
533 Hurricane Irma over the State of Florida. In *Forensic Engineering 2018: Forging Forensic Frontiers*, pages 1028–1038. American Society of
534 Civil Engineers Reston, VA.
535
- 536 Powell, M. D., Houston, S. H., Amat, L. R., and Morisseau-Leroy, N. (1998).
537 The HRD real-time hurricane wind analysis system. *Journal of Wind
538 Engineering and Industrial Aerodynamics*, 77:53–64.
- 539 Powell, M. D., Vickery, P. J., and Reinhold, T. A. (2003). Reduced drag coeffi-
540 cient for high wind speeds in tropical cyclones. *Nature*, 422(6929):279–
541 283.
- 542 Röhrs, J., Christensen, K. H., Hole, L. R., Broström, G., Drivdal, M., and
543 Sundby, S. (2012). Observation-based evaluation of surface wave
544 effects on currents and trajectory forecasts. *Ocean Dynamics*, 62(10–
545 12):1519–1533.
- 546 Schott, F. A., Lee, T. N., and Zantopp, R. (1988). Variability of structure and
547 transport of the Florida Current in the period range of days to seasonal.
548 *Journal of Physical Oceanography*, 18(9):1209–1230.
- 549 Shinn, E. A. (1988). The geology of the Florida Keys. *Oceanus*, 31(1):46–53.
- 550 Siadatmousavi, S. M., Jose, F., and Stone, G. (2011). Evaluation of two WAM
551 white capping parameterizations using parallel unstructured SWAN
552 with application to the Northern Gulf of Mexico, USA. *Applied Ocean
553 Research*, 33(1):23–30.
- 554 Sikirić, M. D., Roland, A., Janečković, I., Tomazić, I., and Kuzmić, M. (2013).
555 Coupling of the Regional Ocean Modeling System (roms) and Wind
556 Wave Model. *Ocean Modelling*, 72:59–73.
- 557 Smith, N. P. (1982). Response of Florida Atlantic shelf waters to hurricane
558 David. *Journal of Geophysical Research: Oceans*, 87(C3):2007–2016.
- 559 Stokes, G. G. (1880). On the theory of oscillatory waves. *Transactions of
560 the Cambridge philosophical society*.

- 561 Tolman, H. L. et al. (2009). User manual and system documentation of
562 WAVEWATCH III TM version 3.14. *Technical note, MMAB Contribution*,
563 276:220.
- 564 Van Den Bremer, T. and Breivik, Ø. (2018). Stokes drift. *Philosophical Trans-*
565 *actions of the Royal Society A: Mathematical, Physical and Engineering*
566 *Sciences*, 376(2111):20170104.
- 567 Villas Bôas, A. B., Cornuelle, B. D., Mazloff, M. R., Gille, S. T., and Arduin,
568 F. (2020). Wave–current interactions at meso-and submesoscales:
569 Insights from idealized numerical simulations. *Journal of Physical*
570 *Oceanography*, 50(12):3483–3500.
- 571 Weisberg, R., Liu, Y., and Mayer, D. (2009). Mean circulation on the west
572 Florida continental shelf observed with long-term moorings. *Geophys.*
573 *Res. Lett*, 36:L19610.
- 574 Weisberg, R. H. and Zheng, L. (2006). Hurricane storm surge simulations
575 for Tampa Bay. *Estuaries and Coasts*, 29(6):899–913.
- 576 Wu, L., Chen, C., Guo, P., Shi, M., Qi, J., and Ge, J. (2011). A FVCOM-
577 based unstructured grid wave, current, sediment transport model, I.
578 Model description and validation. *Journal of Ocean University of China*,
579 10(1):1–8.
- 580 Xian, S., Feng, K., Lin, N., Marsooli, R., Chavas, D., Chen, J., and Hatzikyri-
581 akou, A. (2018). Brief communication: Rapid assessment of damaged
582 residential buildings in the Florida Keys after Hurricane Irma. *Natural*
583 *Hazards and Earth System Sciences*, 18(7):2041–2045.
- 584 Zhang, C., Durgan, S. D., and Lagomasino, D. (2019). Modeling risk of man-
585 groves to tropical cyclones: A case study of Hurricane Irma. *Estuarine,*
586 *Coastal and Shelf Science*, 224:108–116.